RSC Advances

PAPER

View Article Online
View Journal | View Issue

Cite this: *RSC Adv.*, 2019, **9**, 32826

The phase transfer effect of sulfur in lithium–sulfur batteries†

Ziyi Deng,‡[a] Lei Sun,‡[a] Yan Sun,[b] Chunhui Luo,[a] Qiang Zhao *[a] and Kangping Yan[a]

Received 11th September 2019
Accepted 8th October 2019

DOI: 10.1039/c9ra07291h

rsc.li/rsc-advances

Lithium–sulfur (Li–S) batteries are considered to be among the most promising energy storage technologies owing to their high theoretical capacity (1675 mA h g^{-1}). At present, however, discharge mechanisms are complicated and remain a controversial issue. In this work, elemental sulfur, used as an electrical insulator for the cathode, was introduced into batteries for its potential chemical reactions in the electrolyte. A film, prepared by loading elemental sulfur onto glass fiber, was introduced as an interlayer in a Li–S battery. The results demonstrate that elemental sulfur may be reduced to polysulfides even when it functions as an electrical insulator for the cathode. Furthermore, it can improve the overall capacity of the Li–S battery and cycle life. This was verified by simulating the phase equilibrium of the chemical system in Li–S batteries using HSC Chemistry software. We hypothesize that the insulating elemental sulfur could be reduced by polysulfides generated on the cathode, after which they are dissolved in the electrolyte and participate in cathode reactions. This phase transfer effect of sulfur in Li–S batteries revealed a chemical equilibrium in the electrolyte of the Li–S battery, which may form a chemical path embedded into the discharge process of Li–S batteries.

1. Introduction

Lithium–sulfur (Li–S) batteries are considered to be one of the most promising next-generation battery technologies owing to their extremely high theoretical energy density (2600 W h kg^{-1}), excellent environmental protection, and low cost.[1,2] The overall cathode reaction can be described as $S_8 + 16e^- + 16Li^+ \leftrightarrow 8Li_2S$. The discharge mechanism of Li–S batteries, however, is complicated and remains controversial.[3,4] The reduction process of elemental sulfur in these batteries involves a series of miscellaneous chemical reactions and couples of intermediate products.[5,6] It was believed that the molecular ring of S_8 was opened at the beginning of the discharge, generating high-grade polysulfides, such as Li_2S_8 and Li_2S_6[7]. These could be further reduced to short-chain polysulfides, able to be determined by multiple techniques, including Raman spectroscopy,[8,9] UV-Vis spectroscopy,[10] and electrochemical methods.[7] Wen *et al.* observed Li_2S_8, Li_2S_4, Li_2S_2, and Li_2S during the discharge process of the batteries using *in situ* Raman spectroscopy and *in situ* XRD.[11] Polysulfide mono-anions were also confirmed in the chemical system of the Li–S battery. Hagen *et al.* proposed the presence of S^{3-} based on DFT calculations and *in situ* Raman measurements.[8] It was believed that short-chain polysulfides were soluble in the electrolyte; thus, some researchers considered the Li–S battery as a flow battery.[12] The diversity of intermediate species and their specific properties mean that the electrolyte of Li–S batteries is a complex chemical system.[13]

Until now, a large quantity of research still focused on electrochemical reduction processes on the cathode.[14,15] However, conductivity is another dominant factor in the discharging process due to the highly insulating nature of sulfur (5×10^{-30} S cm^{-1} at 25 °C).[16] In the present work, we focus on the behavior of the elemental sulfur electrically isolated in the cathode during the discharging and charging processes of the Li–S battery. A glass fiber was used as the elemental sulfur host, enabling it to be kept isolated from the cathode. The influence of elemental sulfur insulation on the overall capacity and cycle life of batteries was studied, as was how elemental sulfur influences battery performance. The latter was investigated by chemical analysis and thermodynamic simulation. This work aims to understand the mechanism in the above processes.

2. Materials and methods

2.1 Materials

Carbon disulfide (CS_2) and elemental sulfur were purchased from Chengdu Kelong Chemicals Co., Ltd. (Chengdu, China). Glass fiber film was purchased from Whatman Crop. (Kent, UK). Unless otherwise noted, all chemicals were used as received without further purification, and Milli-Q water (18.2 MΩ cm, Millipore System Inc.) was used throughout this study.

[a]*School of Chemical Engineering, Sichuan University, Chengdu 610065, China. E-mail: scuzq@scu.edu.cn*

[b]*School of Mechanical Engineering, Chengdu University, Chengdu 610106, China*

† Electronic supplementary information (ESI) available. See DOI: 10.1039/c9ra07291h

‡ These authors contributed equally to this work.

2.2 Preparation of sulfur-modified glass fiber interlayer (S-GFI)

S-GFI film was prepared using a drop-coating method. For typical preparation, 10 g of elemental sulfur was added to 100 ml of CS_2 and stirred. The as-solution obtained was dropped onto glass fiber films with a diameter of 13 mm using a pipette and dried in a vacuum oven for 12 h at 60 °C before being used in Li–S batteries.

2.3 Electrochemical measurement

Coin-type (CR2025) cells were assembled using S-GFI film to enable the testing of its performance in Li–S batteries. All cells were assembled in an Ar-filled glove box with Li metal as the counter electrode. 1 M lithium bis(trifluoromethanesulfonyl) imide (LiTFSI) in 1,3-dioxolane and 1,2-dimethoxyethane (volume ratio, 1 : 1) was used as the electrolyte, with 1 wt% $LiNO_3$ as an additive. Galvanostatic discharge and charge tests were performed using a cycler (BTS3000, Neware Technology) at various current densities over a potential range of 1.7–2.8 V *vs.* Li^+/Li. The working electrodes were prepared by mixing 80 wt% sulfur/carbon composite, 10 wt% Super-P, and 10 wt% polyvinylidene fluoride (PVDF) binder in *N*-methyl-2-pyrrolidone (NMP). The sulfur content in this sulfur/carbon composite was determined to be approximately 44 wt% by TG analysis as shown in Fig. S1.† The sulfur loading of the electrode ranged from 0.4 to 0.8 mg cm^{-2}.

Morphology was investigated using scanning electron microscopy (S-4800 SEM operating at 5 kV). Raman analysis was conducted using Raman spectrometry (Horiba HR equipped with a 532 nm green laser). Thermogravimetric analysis (TGA) was conducted using Mettler Toledo TGA analyzer (TGA/DSC2) at a heating rate of 10 °C min^{-1} and an argon flow rate of 100 mL min^{-1}.

2.4 Thermodynamic simulation analysis

The behavior of elemental sulfur on the chemical equivalent of polysulfides in the electrolyte was also studied using thermodynamic simulation analysis. The equilibrium composition of the reaction system was simulated using HSC Chemistry 6.0 software. The criterion employed for the simulation was the minimization of Gibbs free energy according to two hypotheses. The first hypothesis is that all of the input substances are considered to be ideal substances and that two or more substances are assumed to be mixed entirely when they can be defined as the same phase. The second hypothesis is that the initial system finally reaches equilibrium. The thermodynamic data used to calculate enthalpy changes in the reactions are shown in Table 1.[17,18]

Table 1 Thermodynamic properties of S_n^{2-} used in the simulation[17,18]

S_n^{2-}	$n=2$	$n=3$	$n=4$	$n=5$	$n=6$	$n=7$	$n=8$
ΔG_f^0, kJ mol^{-1}	77.4	71.1	67.1	66.0	67.4	70.0	74.9
ΔH_f^0, kJ mol^{-1}	18.4	6.6	9.0	9.6	13.3	16.5	23.8
S_f^0, J mol^{-1}	−22	9	63	100	139	171	213

3. Results and discussion

Firstly, a coin-type cell assembly was developed to investigate the electrochemical behavior of the insulating elemental sulfur in Li–S batteries by introducing the as-synthesized S-GFI as a separator. In this battery, two Celgard 2400 films were separately assembled on both sides of S-GFI to avoid the direct electric contraction between S-GFI and cathode, as shown in Fig. 1(a). This battery assembly was termed S–C/Celgard/S-GFI/Celgard/Li. Voltage profiles of its discharging and charging tests are shown in Fig. 1(b and c). The S-GFI film used in this work was prepared using a drop-coating method. The digital image of the as-prepared S-GFI film is presented in Fig. S2,† and SEM micrographs are shown in Fig. S3.† The S-GFI film exhibits a yellow color (Fig. S2†), and elemental sulfur is shown to aggregate as irregular particles among the glass fibers as shown in Fig. S3.† The control experiment was performed as a battery using a glass fiber film without any sulfur, and its voltage profiles was sown in Fig. S4.† As for this battery, approximately 25.5 mg sulfur was loaded onto one S-GFI layer, larger than that loaded on the cathode (~0.8 mg), the sulfur distribution was set to magnify the effect of sulfur on S-GFI. This battery delivered a high reversible maximum capacity of approximately 2600 mA h g^{-1} (calculated on the mass of sulfur loaded on cathode), and about 80 mA h g^{-1} (based on the overall mass of sulfur in this battery, including both the sulfur loaded on the cathode and that on S-GFI film). As known to all, the theoretical capacity of sulfur is 1673 mA h g^{-1}. Obviously, the specific capacity of the battery calculated on the mass of sulfur loaded on cathode (2600 mA h g^{-1}) exceed the theoretical capacity of sulfur. It indicates that the elemental sulfur loaded on the S-GFI film contribute to the capacity of the Li–S battery. In other words, the insulating sulfur loaded on the S-GFI film can participate in the reactions that occurred on the cathode of Li–S battery. Also, take the sulfur loaded on the S-GFI layer into consideration, its specific capacity was about 80 mA h g^{-1}, which indicates that this result did not break the fundamental law and theory in Li–S battery.

The possible reason for the effect was that elemental sulfur loaded on the S-GFI film may have been transferred to the cathode and, thus, was able to participate in electrochemical reactions on the cathode. Loading of elemental sulfur onto S-GFI in Li–S batteries were the key to understanding why this process improves battery properties. To figure out this issue, a Li–S battery equipped with an S-GFI layer was disassembled after being cycled for 140 h, and the S-GFI film, Celgard separator, and Li electrode were collected (Fig. S5†). As shown in Fig. S5(b–d),† both the S-GFI and Celgard separator exhibited a yellow color, probably resulting from soluble polysulfides in the electrolyte, which can be dissolved and spread in electrolyte. In the case of the cycled S-GFI interlayer, the side closer to the cathode showed a deeper yellow color than that closer to the Celgard separator, indicating a higher polysulfide concentration closer to the cathode. Although soluble polysulfides can spread through the electrolyte during cycling, the lithium metal anode still has a fresh metal surface after around 140 h. This

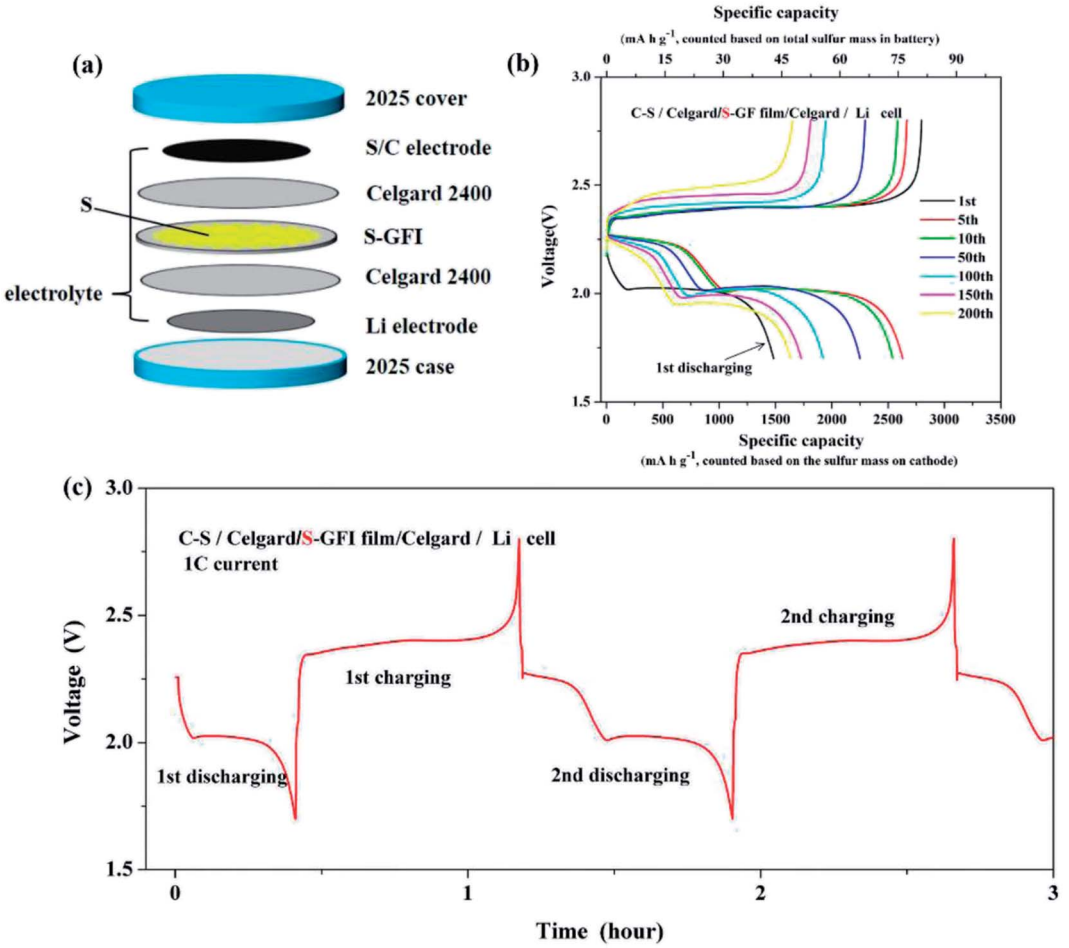

Fig. 1 The cell assembly with S-GFI film and two Celgard 2400 separators (a) and its discharging and charging voltage profiles (b–c).

shows that serve corrosion reactions did not occur on lithium metal in the Li–S battery with an S-GFI film.

Additional work was undertaken to determine the processes occurring on the S-GFI film during cycling. The Li–S battery with an S-GFI film was disassembled after discharging with a C/100 rate, and its S-GFI interlayer was collected. A digital image of this S-GFI interlayer is shown in Fig. 2(a), and corresponding SEM images are shown in Fig. S6.† The discharged S-GFI film exhibits a brown color (Fig. 2(a)) with some aggregates among the glass fibers having a weblike shape as shown in the SEM images. The brown substance may be dissolved in the electrolyte of the batteries, and the obtained solution is shown in Fig. 2(d). This solution also had a brown color, potentially polysulfides dissolved in the electrolyte, according to previous reports in the literature.[19,20] Energy-dispersive spectroscopy analysis was carried out to study the composition of the brown substance on the discharged S-GFI film (Fig. 2(c) and S7†). According to elemental mapping analysis, only Si, O, Na, and S were detected on the discharged S-GFI film. Na, Si, and O may have been sourced from the glass fiber, whereas S may have originated from the brown substance produced during the discharging of Li–S battery.

Moreover, Raman microspectroscopy was conducted to determine the composition of the brown substance, and its results are shown in Fig. 2(e). For these analyses, a homemade chamber was manufactured to prevent sample exposure to the atmosphere during testing, and a quartz window was equipped for laser transmission. The brown solution, obtained by dissolving the discharged S-GFI in the electrolyte, was dropped onto a quartz wafer and dried in a glove box filled with argon. The peak located at 748.8 cm^{-1} beside the signal from elemental sulfur can be assigned to polysulfide (Li_2S_n, n = 4–8)[9,21] (Fig. 2(e)). The elemental sulfur signal may result from elemental sulfur dispersed in the electrolyte during the dissolving process or generated during the drying process, implying that the elemental sulfur (S_8) coating on the S-GFI film was reduced to soluble polysulfides (Li_2S_n) during the discharging of the Li–S battery.

Based on the above analysis, it was found that the S_8 coating on the S-GFI film could be reduced to soluble polysulfides during the discharging of the battery, making it possible to diffuse further into the electrolyte and participate in electrochemical reactions on the cathode. In Fig. 3, we propose a hypothesis to understand the role of the insulating elemental sulfur in the Li–S battery. Firstly, polysulfides were generated on

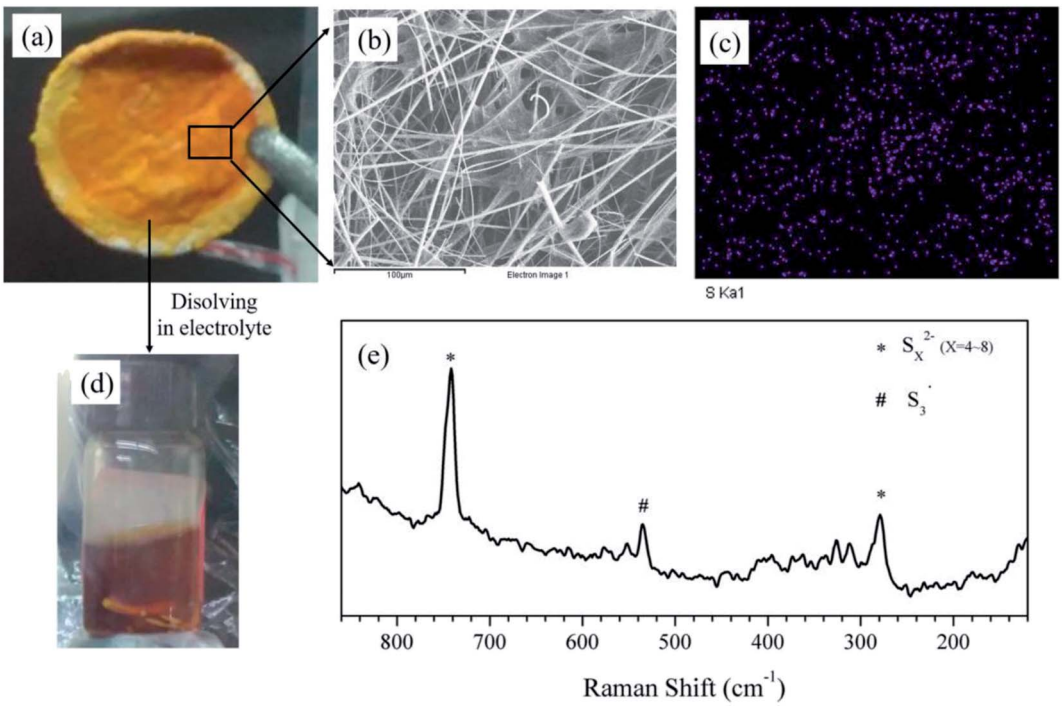

Fig. 2 (a) Digital images of the S-GFI film after discharging in the Li–S battery, (b) SEM image of the discharged S-GFI film, (c) elemental mapping analysis of S in the selected area, (d) the solution after immersing the discharged S-GFI film in the electrolyte, and (e) its Raman spectra.

the cathode during the discharging of the Li–S battery. During this process, elemental sulfur on the cathode was reduced to high-order polysulfides (S_{n1}^{2-}) and low-order polysulfides (S_{n2}^{2-}), successively. These polysulfides can be dissolved and then diffused in the electrolyte, after which they come into contact with the S-GFI film. Elemental sulfur on the S-GFI film may react with low-order polysulfides and generate high-order polysulfides according to eqn (1), which was previously reported by Shin-Ichi Tobishima and colleagues.[22] This effect may help to explain how the S-GFI interlayer improved overall capacity.

$$S_8 + S_{n2}^{2-} \rightarrow S_{n1}^{2-} \ (1 \leq n2 \leq n1 \leq 8) \quad (1)$$

The equilibrium composition of polysulfides in the Li–S battery system was simulated using HSC Chemistry 6.0 software. This simulation analysis was based on the following assumptions. Firstly, mono-anion species were not taken into account in the simplification of this simulation. All polysulfide anions (S_n^{2-}, $1 \leq n \leq 8$) and elemental sulfur were then set as possible components in this chemical system. Secondly, enough solvent (DME) was preset in this simulation to reduce

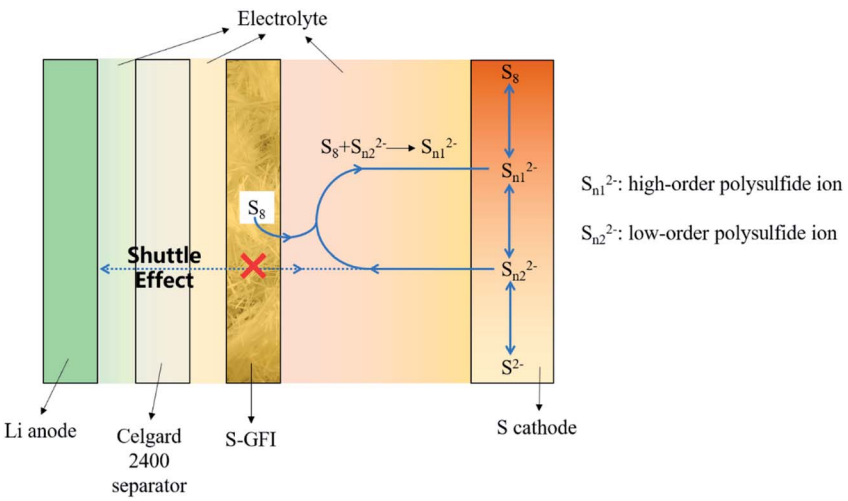

Fig. 3 Schematic showing the role of elemental sulfur loaded onto S-GFI film in Li–S batteries.

the impact of the solubility of certain species. Thirdly, the temperature of the system was fixed at 25 °C to ignore the influence of temperature fluctuation. The equilibrium amount of species in this system with a varying initial amount of elemental sulfur was calculated in order to simulate the reaction between elemental sulfur and polysulfides generated during the discharge of the battery. In the simulated system, the discharging depth was fixed by setting a 2 mol electron transfer for the electrochemical reactions. The results of the simulation are shown in Fig. 4 and indicate that elemental sulfur was reduced to S^{2-} when the addition of sulfur was less than 1/8 mol. The amount of polysulfides, including S^{2-}, S_2^{2-}, S_3^{2-}, S_4^{2-}, S_5^{2-}, S_6^{2-}, S_7^{2-}, and S_8^{2-}, increased with increasing elemental sulfur addition. The amount of S_6^{2-}, S_7^{2-}, and S_8^{2-} was found to be lower than that of the low-grade polysulfides. This result indicated that low-grade polysulfides generated in the discharging process could be transformed into high-grade polysulfides upon reaction with elemental sulfur. The simulation results served to verify the hypotheses concerning the role of elemental sulfur in the Li–S battery. A complex chemical equilibrium between polysulfides and elemental sulfur was also noted. Some previous research has considered chemical equilibrium in the electrolyte of Li–S batteries, for example, Hengliang and colleagues noted that several polysulfides existed in the electrolyte of Li–S battery after *in situ* Raman spectroscopy analyses.[23] Based on this result, it seems difficult to make a pure polysulfide solution with a prescribed chain length but rather a mixture of several polysulfides.

Based on the phase diagram shown in Fig. 4, a serious of potential chemical reactions occurred in this system and are listed in Table 2. As shown in Table 2, the reactions between elemental sulfur and low-grade sulfides (S^2, S_2^{2-}, and S_3^{2-}) have negative ΔG and ΔH and large chemical equilibrium constants, indicating that these reactions were spontaneous thermodynamic processes. This result confirmed the hypothesis that elemental sulfur could be reduced to high-grade polysulfides in Li–S batteries. However, as the chain length of the polysulfides in the reactant increased, the reactions showed higher ΔG and ΔH and a decreased equilibrium constant, indicating the reversible nature of the reactions. Based on these results, we suggest that low-grade polysulfides could be easily transferred to high-grade polysulfides, whereas high-grade polysulfides maintained a preferred chemical balance even if more elemental sulfur was introduced.

Through the above reactions, the elemental sulfur loaded on the glass fiber could be reduced by low-grade polysulfides to high-grade polysulfides. The high-grade polysulfides generated in this process may be dissolved and diffused in the electrolyte of a Li–S battery, and this effect could increase the soluble polysulfide concentration in the electrolyte, especially near the cathode. The results of this analysis fit perfectly the distribution of polysulfide ions shown in Fig. 4. Therefore, a battery equipped with an S-GFI film can act as a flow battery, whereas its catholyte can obtain extra polysulfides from the S-GFI film through a series of chemical reactions. Further to this, the dissolved polysulfides from these reactions can transfer to the cathode surface and be reduced to Li_2S and Li_2S_2 electrochemically. Objectively speaking, the elemental sulfur loaded onto the S-GFI film, which is electrically insulated to the cathode and cannot be dissolved directly into the electrolyte, was transferred to the electrode and electrochemically reduced. Additionally, the elemental sulfur started with the solid phase on the S-GFI film and was transferred to a solution phase in the electrolyte as polysulfides and reduced electrochemically to insoluble solid phases on the cathode (Li_2S and Li_2S_2). We have termed this effect the "phase transfer effect of sulfur" for Li–S batteries. Due to this phase transfer effect, the elemental sulfur that was insulated to the cathode can be utilized and can participate in the electrode reaction on the cathode.

Basically, elemental sulfur has low electrical conductivity, which is commonly hot-melt with porous carbon to increase the conductivity of the cathode materials in a Li–S battery. It is possible that some elemental sulfur aggregates may give rise to local low-conductivity areas and provide a possible reason for which the specific capacity of the S/C composites was only about 1200 mA h g^{-1} even in the first cycle, as shown in Fig. S4.† According to the theory of phase transfer, elemental sulfur can be transferred to polysulfides as long as it is in contact with the electrolyte of the Li–S battery. Insulated elemental sulfur was chemically reduced to polysulfides and dissolved in catholyte, then transported to the cathode surface with good electric contact with the electrode through a solution path, at which point it is able to participate in cathodic electrochemical reactions. This theory introduces "a chemical path" into the cathode reaction process, making it possible to discharge even when elemental sulfur acts as an electrical insulator to the cathode. Elemental sulfur can also be introduced to the battery beyond the cathode, according to the theory of phase transfer effect. Herein, the elemental sulfur loaded on the S-GFI film was approximately 20-fold as much that loaded on the cathode, which was too great to be loaded entirely onto the cathode as an S/C composite. This provides a possible method for the development of Li–S batteries with high elemental sulfur loading.

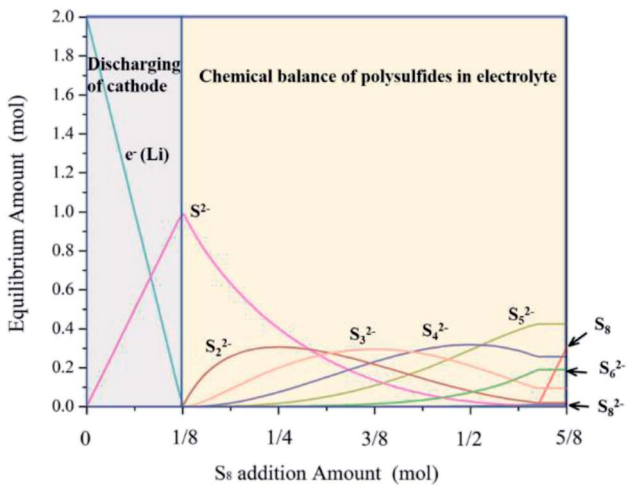

Fig. 4 The influence of elemental sulfur addition on the equilibrium amount of the polysulfide species in this chemical system.

Table 2 The possible reactions and their thermodynamic parameters

Reactant polysulfides	Reaction	Delta H kJ mol^{-1}	Delta S J °C^{-1} mol^{-1}	Delta G kJ mol^{-1}	Equilibrium constant K
S^{2-}	$S^{2-} + 1/8S_8 = S_2^{2-}$	−20.095	−39.468	−8.328	2.879
	$S^{2-} + 1/4S_8 = S_3^{2-}$	−26.495	−40.538	−14.409	334.700
	$S^{2-} + 3/8S_8 = S_4^{2-}$	−24.095	−18.608	−18.548	177.700
	$S^{2-} + 1/2S_8 = S_5^{2-}$	−23.495	−13.678	−19.417	252.400
	$S^{2-} + 5/8S_8 = S_6^{2-}$	−19.795	−6.748	−17.784	1306.000
	$S^{2-} + 3/4S_8 = S_7^{2-}$	−16.595	−6.818	−14.563	356.100
	$S^{2-} + 7/8S_8 = S_8^{2-}$	−9.295	3.112	−10.223	61.840
S_2^{2-}	$S_2^{2-} + 1/8S_8 = S_3^{2-}$	−6.400	−1.070	−6.081	11.630
	$S_2^{2-} + 1/4S_8 = S_4^{2-}$	−4.000	20.860	−10.219	61.740
	$S_2^{2-} + 3/8S_8 = S_5^{2-}$	−3.400	25.790	−11.089	87.690
	$S_2^{2-} + 1/2S_8 = S_6^{2-}$	0.300	32.720	−9.455	45.360
	$S_2^{2-} + 5/8S_8 = S_7^{2-}$	3.500	32.650	−6.235	12.370
	$S_2^{2-} + 3/4S_8 = S_8^{2-}$	10.80	42.580	−1.895	2.148
S_3^{2-}	$S_3^{2-} + 1/8S_8 = S_4^{2-}$	2.400	21.930	−4.138	5.310
	$S_3^{2-} + 1/4S_8 = S_5^{2-}$	3.000	26.860	−5.008	7.542
	$S_3^{2-} + 3/8S_8 = S_6^{2-}$	6.700	33.790	−3.375	3.902
	$S_3^{2-} + 1/2S_8 = S_7^{2-}$	9.900	33.720	−0.154	1.064
	$S_3^{2-} + 5/8S_8 = S_8^{2-}$	17.200	43.650	4.186	1.848
S_4^{2-}	$S_4^{2-} + 1/8S_8 = S_5^{2-}$	0.600	4.930	−0.870	1.420
	$S_4^{2-} + 1/4S_8 = S_6^{2-}$	4.300	11.860	0.764	0.735
	$S_4^{2-} + 3/8S_8 = S_7^{2-}$	7.500	11.790	3.985	0.200
	$S_4^{2-} + 1/2S_8 = S_8^{2-}$	14.800	21.720	8.324	0.035
S_5^{2-}	$S_5^{2-} + 1/8S_8 = S_6^{2-}$	3.700	6.930	1.634	0.517
	$S_5^{2-} + 1/4S_8 = S_7^{2-}$	6.900	6.860	4.855	0.141
	$S_5^{2-} + 3/8S_8 = S_8^{2-}$	14.200	16.790	9.194	0.025
S_6^{2-}	$S_6^{2-} + 1/8S_8 = S_7^{2-}$	3.200	−0.070	3.221	0.273
	$S_6^{2-} + 1/4S_8 = S_8^{2-}$	10.500	9.860	7.560	0.047
S_7^{2-}	$S_7^{2-} + 1/8S_8 = S_8^{2-}$	7.300	9.930	4.339	0.174

Based on the findings of this work, the introducing of sulfur loaded interlayer in battery can act as a promising method to enhance the overall capacity for Li–S battery. Herein, a Li–S battery assembly, with an S-GFI and a Celgard separator assembled between the S-GFI film and lithium metal anode, was built and labeled as S–C/S-GFI/Celgard/Li. Its voltage profiles and cycle performance are shown in Fig. 5, indicating that the specific capacity of S–C/S-GFI/Celgard/Li was maintained at 2000 mA h g^{-1} (based on sulfur loaded onto the cathode). The control experiment for a Li–S battery without any S-GFI separator was also performed. The specific capacity for the control test was about 1200 mA h g^{-1} for the first discharge and decreased to about 500 mA h g^{-1} after 100 cycles. In this work, all the cathode used in the above batteries was selected with similar sulfur loading density. So, the overall capacity of this battery was increased about four times as the introducing of the S-GFI film. This demonstrates that the S-GFI film can quadruple the overall capacity of the battery without increasing its weight remarkably. Moreover, the S–C/S-GFI/Celgard/Li battery was able to maintain a specific capacity of

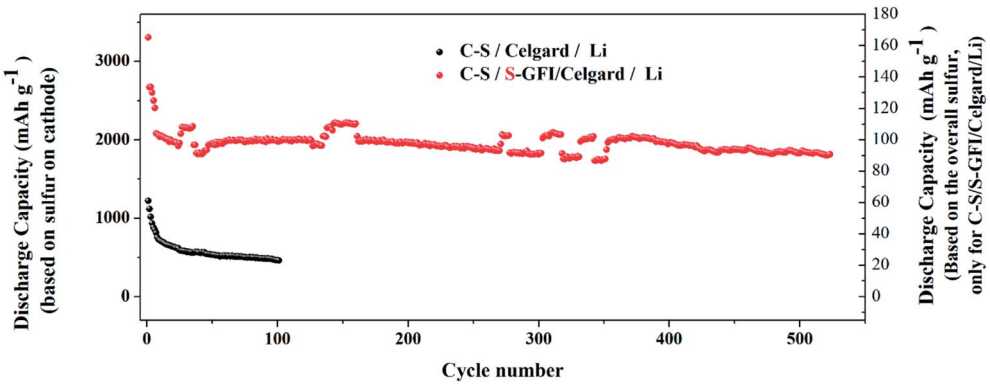

Fig. 5 The cycle performance comparison between C–S/Celgrad/Li cell and C–S/S-GFI film/Celgrad/Li cell.

2000 mA h g^{-1} even when cycled more than 500 times. However, considering that the elemental sulfur was loaded onto the S-GFI film, the specific capacity was only about 100 mA h g^{-1}. Also, it was noted that the cell assembly with S-GFI film and two Celgard 2400 separators exhibited an increased voltage difference between the discharging and charging platform. This difference was approximately 0.4 V for the battery with the S-GFI film but only around 0.2 V for the battery without S-GFI film. We suggest that this voltage difference was caused by the charge transfer resistance introduced by the Celgard separator.

4. Conclusion

In this work, the behavior of electrically insulated elemental sulfur in Li–S batteries was investigated by introducing an elemental sulfur-modified glass fiber interlayer (S-GFI) between the elemental sulfur and the cathode. It was found that the insulated elemental sulfur improves the capacity and lifespan of Li–S batteries (its initial reversible capacity reaches 2600 mA h g^{-1} while retaining 1800 mA h g^{-1} after 500 cycles). Furthermore, elemental sulfur loaded onto the S-GFI interlayer was found to reduce to soluble polysulfides during the discharging process of Li–S batteries. HSC Chemistry software was employed to simulate the influence of elemental sulfur on the chemical balance in Li–S batteries. The results confirmed that the insulating elemental sulfur in a Li–S battery could be reduced to high-grade polysulfides by low-grade polysulfides from the cathode, after which they could participate in the discharging process of the Li–S battery. This process was termed the phase transfer effect of sulfur in the Li–S battery and may reveal a chemical polysulfides system in the electrolyte of Li–S batteries.

Conflicts of interest

There are no conflicts to declare.

Acknowledgements

We gratefully acknowledge the financial support from the National Natural Science Foundation of China (Grant No. 51702027) and the Opening Project of Material Corrosion and Protection Key Laboratory of Sichuan province (Grant No. 2017CL19). Help from the Analytical & Testing Center of Sichuan University is also greatly appreciated.

Notes and references

1 Y. Fu and A. Manthiram, *RSC Adv.*, 2012, **2**, 5927–5929.
2 S. Chen, F. Dai, M. L. Gordin and D. Wang, *RSC Adv.*, 2013, **3**, 3540–3543.
3 Z. Wen, A. Paolella, C. S. Kim, Z. Feng, L. Dong, C. Gagnon, J. Trottier, G. Abdelbast, A. Vijh and A. Mauger, *Sustainable Energy Fuels*, 2017, **1**, 737–747.
4 H. Wei, J. Ma, B. Li, Y. Zuo and D. Xia, *ACS Appl. Mater. Interfaces*, 2014, **6**, 20276–20281.
5 D. Zheng, X. Zhang, J. Wang, D. Qu, X. Yang and D. Qu, *J. Power Sources*, 2016, **301**, 312–316.
6 L. A. Huff, J. L. Rapp, J. A. Baughman, P. L. Rinaldi and A. A. Gewirth, *Surf. Sci.*, 2014, **631**, 295–300.
7 M. J. Lacey, K. Edström and D. Brandell, *Electrochem. Commun.*, 2014, **46**, 91–93.
8 M. Hagen, P. Schiffels, M. Hammer, S. Dörfler, J. Tübke, M. J. Hoffmann, H. Althues and S. Kaskel, *J. Electrochem. Soc.*, 2013, **160**, A1205–A1214.
9 W. Heng-Liang, L. A. Huff and A. A. Gewirth, *ACS Appl. Mater. Interfaces*, 2015, **7**, 1709–1719.
10 H. Marceau, C. S. Kim, A. Paolella, S. Ladouceur, M. Lagacé, M. Chaker, A. Vijh, A. Guerfi, C. M. Julien and A. Mauger, *J. Power Sources*, 2016, **319**, 247–254.
11 W. Zhu, A. Paolella, C. S. Kim, D. Liu, Z. Feng, C. Gagnon, J. Trottier, A. Vijh, A. Guerfi, A. Mauger, C. M. Julien, M. Armand and K. Zaghib, *Sustainable Energy Fuels*, 2017, **1**, 737–747.
12 J. Li, L. Yang, B. Yuan, G. Li and J. Y. Lee, *Materials Today Energy*, 2017, **5**, 15–21.
13 M. Gu, J. Lee, Y. Kim, J. S. Kim, B. Y. Jang, K. T. Lee and B.-S. Kim, *RSC Adv.*, 2014, **4**, 46940–46946.
14 M. Ren, X. Lu, Y. Chai, X. Zhou, J. Ren, Q. Zheng and D. Lin, *J. Colloid Interface Sci.*, 2019, **552**, 91–100.
15 G. D. Park, D. S. Jung, J.-K. Lee and Y. C. Kang, *Chem. Eng. J.*, 2019, **373**, 382–392.
16 N. Osada, C. B. Bucur, H. Aso and J. Muldoon, *Energy Environ. Sci.*, 2016, **9**, 1668–1673.
17 A. Kamyshny, J. Gun, D. Rizkov, T. Voitsekovski and O. Lev, *Environ. Sci. Technol.*, 2007, **41**, 2395–2400.
18 J. P. Amend and E. L. Shock, *FEMS Microbiol. Rev.*, 2001, **25**, 175–243.
19 Z. Du, C. Guo, L. Wang, A. Hu, S. Jin, T. Zhang, H. Jin, Z. Qi, S. Xin, X. Kong, Y. G. Guo, H. Ji and L. J. Wan, *ACS Appl. Mater. Interfaces*, 2017, **9**, 43696–43703.
20 X. Tao, J. Wang, L. Chong, H. Wang, H. Yao, G. Zheng, S. Z. Wei, Q. Cai, W. Li and G. Zhou, *Nat. Commun.*, 2016, **7**, 11203.
21 J.-T. Yeon, J.-Y. Jang, J.-G. Han, J. Cho, K. T. Lee and N.-S. Choi, *J. Electrochem. Soc.*, 2012, **159**, A1308–A1314.
22 S. I. Tobishima, H. Yamamoto and M. Matsuda, *Electrochim. Acta*, 1997, **42**, 1019–1029.
23 H.-L. Wu, L. A. Huff and A. A. Gewirth, *ACS Appl. Mater. Interfaces*, 2015, **7**, 1709–1719.

